Tidal Energy "Round Robin" Tests[☆]
Comparisons between towing tank and circulating tank results

B. Gaurier[a,*], G. Germain[a,*], J.V. Facq[a], C.M. Johnstone[b], A.D. Grant[b], A.H. Day[c], E. Nixon[c], F. Di Felice[d], M. Costanzo[d]

[a] *IFREMER, Marine Structures Laboratory, Boulogne-sur-mer, France*
[b] *University of Strathclyde, Energy Systems Research Unit, Glasgow, UK*
[c] *University of Strathclyde, Kelvin Hydrodynamics Laboratory, Glasgow, UK*
[d] *CNR-INSEAN, Propulsion and Cavitation Laboratory, Rome, Italy*

Abstract

One key step of the industrial development of a tidal energy device is the testing of scale prototype devices within a controlled laboratory environment. At present, there is no available experimental protocol which addresses in a quantitative manner the differences which can be expected between results obtained from the different types of facilities currently employed for this type of testing. As a consequence, where differences between results are found it has been difficult to confirm the extent to which these differences relate to the device performance or to the test facility type.

In the present study, a comparative "Round Robin" testing programme has been conducted as part of the EC FP VII MaRINET program in order to evaluate the impact of different experimental facilities on the test results. The aim of the trials was to test the same model tidal turbine in four different test facilities to explore the sensitivity of the results to the choice of facility. The facilities comprised two towing tanks, of very different size, and two circulating water channels.

Performance assessments in terms of torque, drag and inflow speed showed very similar results in all facilities. However, expected differences between the different tank types (circulating and towing) were observed in the fluctuations of torque and drag measurements. The main facility parameters which can influence the behaviour of the turbine were identified; in particular the effect of blockage was shown to be significant in cases yielding for high thrust coefficients, even at relatively small blockage ratios.

Keywords: "Round Robin" Test, Experimental Trials, Marine Current Energy, Horizontal Axis Marine Turbine

[☆] FP7 - MaRINET "Round Robin"

[*] Corresponding authors

Email addresses: benoit.gaurier@ifremer.fr (B. Gaurier), gregory.germain@ifremer.fr (G. Germain), jean.valery.facq@ifremer.fr (J.V. Facq), cameron.johnstone@strath.ac.uk (C.M. Johnstone), andrew.grant@strath.ac.uk (A.D. Grant), sandy.day@strath.ac.uk (A.H. Day), edward.nixon@strath.ac.uk (E. Nixon), fabio.difelice@cnr.it (F. Di Felice), marcello.costanzo@cnr.it (M. Costanzo)

1. Introduction

Tank testing is primarily undertaken to establish the behaviour of a tidal energy converter at model scale and to identify the impact of different flow conditions, turbine configuration and turbine dimensions on device performance. The availability of a controlled environment where each set of experiments can be repeated is highly valuable. Due to the fact that marine renewable testing centres are not uniformly configured or constructed, standardisation in test practices is an important aspect to MaRINET [1, 2]. At present there is no pan-European or worldwide consensus on appropriate test methodologies and practices to be implemented, even if procedures developed within the EC FP VI EquiMar project [3], have been carried out. Recently, ITTC have adopted international best practice guidelines for tidal turbine testing [4].

Different experimental approaches are used to model the behaviour of horizontal-axis marine current turbines. Solid and porous discs are usually used for small scale trials in order to open up new topics of investigation like in [5], [6] and [7] respectively for flow characterization, and study of device interaction and turbulence effects. These experiments can give, in a first approach, a good understanding of the fluid / structure interaction process; however medium scale studies of rotating turbines taking into account the geometrical characteristics of the device are still needed.

Numerous studies have been carried out in flume tanks in recent years. [8] give interesting results on a single turbine wake development, including turbulence intensity. [9] depicted many turbine performance curves depending on the number of blades, pitch angle, etc. In another study, [10] presented interesting turbine performance and thrust curves, mainly oriented towards blade loads owing to oscillatory flows, similarly to [11] and [12]. Whilst some of those experimental results were used as a basis for numerical-experimental validation such as [13] and [14], none of them follow a standard experimental protocol. So, direct comparisons cannot reliably be made.

[15] carried out a power and thrust coefficient study on a $0.8m$ diameter turbine model in both a towing tank and a cavitation tunnel. Unfortunately, the presented results are complementary and not directly comparable, since the experimental parameters (upstream flow velocities) were not equivalent in both experimental facilities.

In order to evaluate the influence of the use of different experimental tank facilities to tidal turbine performances characterization, a comparative "Round Robin" testing programme has been conducted as part of the EC FP VII MaRINET program. The same tidal turbine model has been tested at four experimental facilities. The facilities used in the testing program include two towing tanks, at CNR-INSEAN (Rome, $220m$ long) and at Strathclyde University (Glasgow, $76m$ long), and two recirculating flume tanks at CNR-INSEAN (Rome) and at IFREMER (Boulogne-sur-mer). The scale tidal turbine used in this comparative testing program is a three bladed horizontal-axis turbine designed by IFREMER as previously tested by [16].

In this paper we report the program of work executed in this "Round Robin" testing program by presenting first the experimental set-up in term of facilities, equipment and instrumentation, and the protocol used for the testing. We will then focus on the comparison of the obtained results in term of power and thrust coefficients in flow velocities ranging from 0.6 to $1.2m/s$. This comparison will be based only on results of performance assessment of the device characterized by rotor torque and thrust measurements.

2. Experimental Facilities and Set-up

This section aims at giving a detailed description of the experimental set-up and measurement facilities used for the experiments. The definitions of the quantities that will be used for the analysis are also presented in this section.

2.1. Experimental facilities

The facilities used in the testing program include two towing tanks, at CNR-INSEAN (Rome, $220m$ long) and at Strathclyde University (Glasgow, $76m$ long), and two recirculating tanks at CNR-INSEAN (Rome) and at IFREMER (Boulogne sur mer). A brief description of these facilities is presented below in table 1.

Laboratory name	IFREMER	KHL	CNR-INSEAN 1	CNR-INSEAN 2
Type of tank	flume	towing	flume	towing
Length $[m]$	18	76	10	220
Width $\times$ depth $[m]$	4×2	4.6×2.5	3.6×2.25	9×3.5
Speed range $[m/s]$	0.1 to 2.2	0.1 to 5	0.3 to 5	0.1 to 10
Turbulence int. [%]	3 to 15	NA	2.5 to 12	NA
Blockage ratio [%]	4.8	3.3	4.8	1.2

Table 1: Testing facilities main characteristics

2.1.1. Towing tank

The CNR-INSEAN towing tank number 2 has been used for these trials. The main dimensions are: $220m \times 9.0m \times 3.5m$, in length, width and depth, respectively.

The Kelvin Hydrodynamics Laboratory (KHL) towing tank of the University of Strathclyde has dimensions of $76m$ length by $4.6m$ width and $2.5m$ depth. Both tanks (Figures 1 and 2) are equipped with a self-propelled towing carriage on which the turbine model is fixed.

The carriage velocity is computer controlled and was ramped up at constant acceleration at the start of each test, and then maintained constant for the duration of the test period before being ramped down for a stop at the end of the tank. The maximum carriage speeds are $5m/s$ and $10m/s$ respectively at KHL and CNR-INSEAN towing tank; both tanks have speed control accurate to better than 0.3%.

Due to the length of the KHL towing tank, only one condition (one carriage speed and one turbine rotation speed) could be tested during a single run, with acquisition duration depending on the carriage speed (Table 2). In the CNR-INSEAN towing tank, it is possible to acquire data at different turbine rotation speeds during one tank run. In this case the minimum acquisition time was fixed to 60 seconds (see section 2.5).

Carriage speed $[m/s]$	0.6	0.8	1.0	1.2
Acquisition time $[s]$	70	50	39	30

Table 2: Acquisition time in function of the carriage velocity, for the KHL towing tank

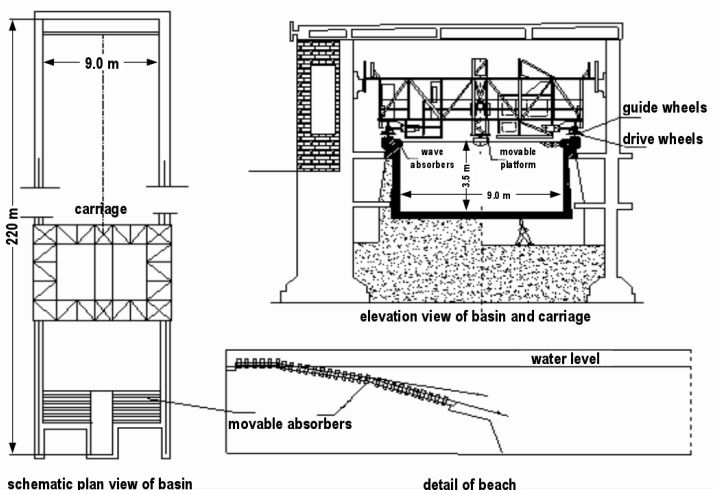

Figure 1: Schematic of the CNR-INSEAN towing tank

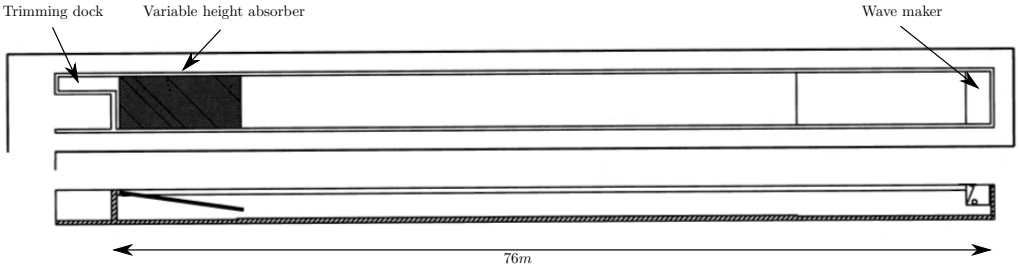

Figure 2: Schematic of the KHL towing tank

2.1.2. Circulating tank

The trials were run in two flume tanks at CNR-INSEAN and at IFREMER. The CNR-INSEAN circulating water channel, depicted in Figure 3, has a working section of $10m$ length by $3.6m$ width and $2.25m$ depth. The streamwise flow velocity range is 0.1 to $5.0m/s$.

The wave and current flume tank of IFREMER, depicted in Figure 4, has a working section of $18m$ length by $4m$ width and $2m$ depth. The streamwise flow velocity range is 0.1 to $2.2m/s$. More details about this flume tank can be found in [17].

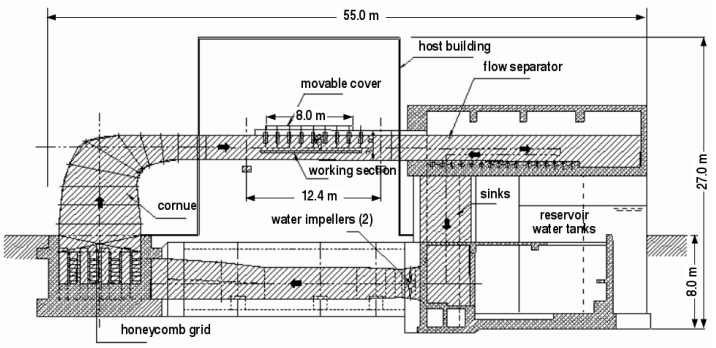

Figure 3: Schematic of the CNR-INSEAN flume tank

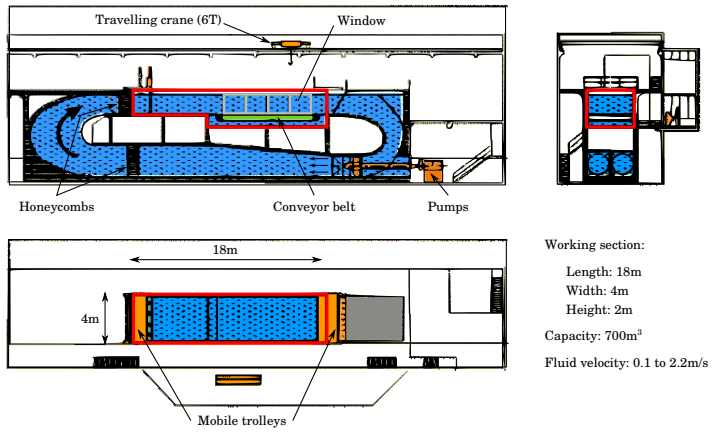

Figure 4: IFREMER's Boulogne-sur-Mer flume tank description

The upstream turbulence intensity rate of the flow I_∞ is defined by:

$$I_\infty = 100\sqrt{\frac{\frac{1}{3}\left[\sigma^2(u_\infty)+\sigma^2(v_\infty)+\sigma^2(w_\infty)\right]}{\bar{u}_\infty^2+\bar{v}_\infty^2+\bar{w}_\infty^2}} \tag{1}$$

where the velocity components u_∞, v_∞, w_∞ are those of the upstream velocity U_∞.

The level of turbulence intensity is of great interest in marine turbine studies, such as [16]. However, whilst it would have been possible to work with different levels of turbulence in both flume tanks, only the lowest ambient turbulence condition has been considered in this work. In order to be as close as possible to the towing tank flow conditions, 2.5% and 3% turbulence intensity levels have been chosen for CNR-INSEAN and IFREMER tanks respectively. Four different upstream velocities (from $U_\infty = 0.6$ to $1.2m/s$) are considered with these I_∞.

2.2. Turbine model description

The model consists of a three-bladed horizontal axis turbine, which is $D = 2R = 0.7m$ in diameter. The rotor is connected to a motor-gearbox assembly consisting of a gearbox, a DC motor, a ballast load and a motor speed control unit, providing an active rotor speed control. The turbine blades are designed from a NACA 63-418 profile (see [18] for profile details). A torque meter is placed between the rotor and the gearbox for torque measurements. A more detailed geometrical description of the blade is given in table 3 and a synthesis view of the turbine is given in figure 5. The same model has been used in all facilities.

r/R	c/R	Pitch (deg)	t/c (%)
0.1333	0.0567	29.5672	80.0
0.1500	0.0567	29.5672	100.0
0.1550	0.0567	29.5672	100.0
0.1983	0.1521	25.6273	36.0
0.2417	0.2474	22.1491	21.3
0.2850	0.2375	19.3031	21.4
0.3283	0.2259	16.9737	21.7
0.3717	0.2141	15.0538	22.0
0.4150	0.2029	13.4572	22.2
0.4583	0.1925	12.1169	22.4
0.5017	0.1829	10.9815	22.5
0.5450	0.1743	10.0114	22.5
0.5883	0.1665	9.1761	22.4
0.6317	0.1594	8.4516	22.2
0.6750	0.1529	7.8191	21.9
0.7183	0.1471	7.2638	21.5
0.7617	0.1418	6.7735	20.9
0.8050	0.1370	6.3387	20.2
0.8483	0.1325	5.9514	19.5
0.8917	0.1285	5.6050	18.6
0.9350	0.1247	5.2941	18.0
0.9783	0.1213	5.0143	18.0
1.0000	0.0655	4.8743	25.0

Table 3: Detailed blade geometrical description with the chord (c), the pitch angle and the thickness (t) in function of the varying radius r

The blockage ratio α is defined as the ratio between the turbine cross-section area $S = \pi R^2$ and the flume tank transverse area $A = WH$:

$$\alpha = \frac{S}{A} = \frac{\pi R^2}{WH} \tag{2}$$

where W and H respectively denote the test section width and depth. α is given in table 1 for every four facilities: the flume tank of IFREMER, the towing tank of KHL, the flume tank of CNR-INSEAN and the towing tank of CNR-INSEAN.

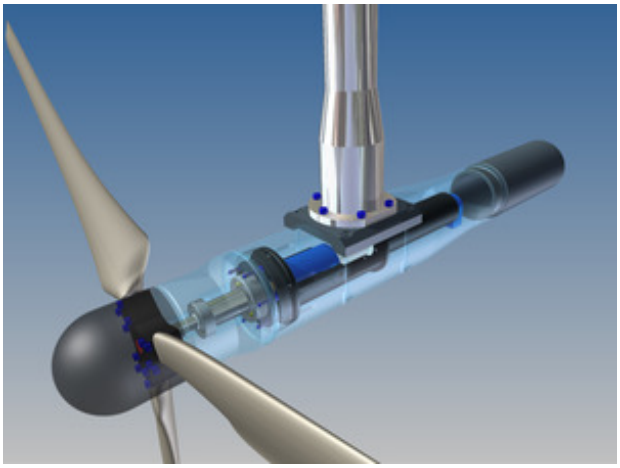

Figure 5: 3D CAD view of the turbine.

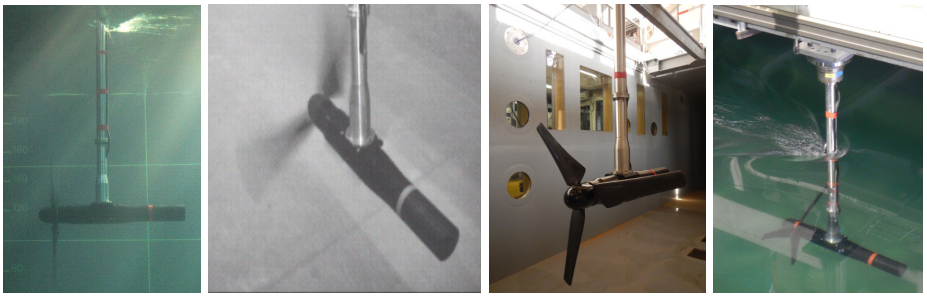

Figure 6: Views of the turbine in the IFREMER flume tank at rest, during a measurement in the KHL towing tank from an underwater camera, in the empty CNR-INSEAN flume tank and during a carriage reverse in the CNR-INSEAN towing tank, from the left to the right.

The Tip Speed Ratio (TSR) is defined as the ratio between the tip velocity and the upstream flow velocity as follow:

$$\mathrm{TSR} = \frac{|\Omega| R}{U_\infty} \tag{3}$$

where Ω is the rotor angular velocity, R is the rotor radius and U_∞ is the upstream flow velocity. In our study, the turbine TSR varies from 0 to 7.

Finally, the radius-based Reynolds number is given by:

$$\mathrm{Re}_\infty = \frac{U_\infty R}{\nu} \tag{4}$$

where ν denotes the fluid kinematic viscosity and is approximately $\nu \simeq 10^{-6}\ m^2 s^{-1}$. The studied Reynolds number range is then directly deduced from the U_∞ range mentioned above, which gives $\mathrm{Re}_\infty \in [140{,}000; 420{,}000]$. A summary description of the structure is presented in table 4.

Profile	NACA 63418
Rotor Radius (R)	$350mm$
Hub Radius	$46mm$
Hub length	$720mm$
Studied TSR	$[0-7]$
Sense of rotation	counter-clockwise
Reynolds (Re_∞)	$[140-420].10^3$

Table 4: Turbine model general description.

2.3. Power and thrust measurements

The forces and moments acting on the structure are obtained by means of a six-component load cell, which measures the three force components and the three moment components, at a $100Hz$ sampling frequency. A torque sensor, directly fixed between the rotor and the motor, provides a more accurate measurement of the axial torque than the one given by the load cell, also at a $100Hz$ sampling frequency.

The power coefficient C_P is defined as the proportion of power P captured by the turbine as compared to the maximum available power P_∞ from the incoming flow through the turbine cross-section area S:

$$C_P = \frac{P}{P_\infty} = \frac{M_x\,\Omega}{\frac{1}{2}\,\rho\,S\,U_\infty^3} \tag{5}$$

where ρ is the fluid density and M_x is the axial moment (torque), defined as the x-component moment.

Similarly, the thrust coefficient C_T is defined as the axial force F_x acting upon the turbine as compared to the kinetic energy of the incoming flow through S:

$$C_T = \frac{F_x}{\frac{1}{2}\,\rho\,\pi\,R^2\,U_\infty^2} \tag{6}$$

The F_x measured here actually includes the axial force on the whole structure, that is the blades, the hub and the mast, since the load-cell is located at the top of the mast to allow easy installation in different facilities. It is widely accepted that C_T is an expression involving rotor thrust only, so C_T presented in this paper are overestimated because drag force on the structure is not subtracted (*e.g.* as already shown in [16] and [19]). It should be noted that one undesirable side effect of this is that the results are sensitive to the exact submersion of the turbine, and hence the length of the submerged part of the mast.

Obviously, the M_x and F_x values used to compute those coefficients are time-averaged values. The measurement (and thus the averaging) duration is $T = 100$ seconds in the two flume tanks of CNR-INSEAN and IFREMER, which provides converged values of C_P and C_T (see section 2.5). In the towing tanks, this measurement duration is not fixed; for the KHL towing tank, it is dependant on the tank length and towing speed as shown in table 2, while for the CNR-INSEAN towing tank, the minimum measurement duration was fixed to 60 seconds.

2.4. Experimental protocol

The acquisition hardware is composed of a signal conditioning chassis equipped with strain gauges analogue inputs. All signals coming from the load-cell, the torque-meter and the motor are recorded with an in-house software package developed by IFREMER staff at a sample frequency of $100Hz$.

In each tank, the turbine depth is kept constant at $1m$ under the free surface (figure 7). The turbine is fixed on a moving carriage in the towing tanks and on a customised mounting in the flume tanks.

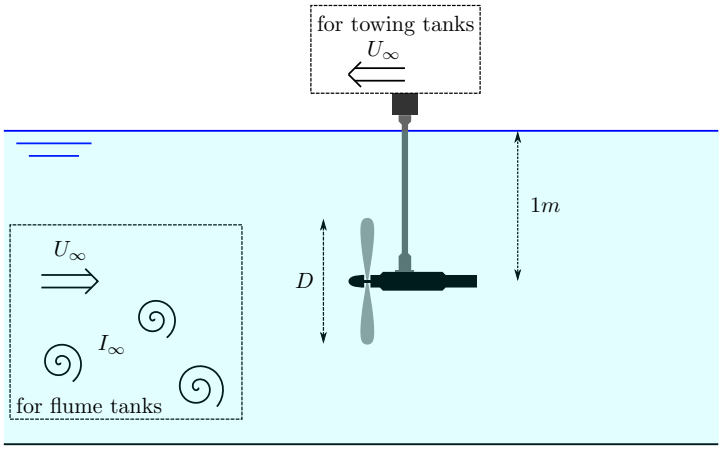

Figure 7: Schematic of the set-up

The flow velocity or carriage velocity is chosen and fixed for each set of tests; the turbine rotation speed is then varied to adjust the tip speed ratio. The rotational speed is measured and controlled for each measurement point, but is adjusted manually. This explains why in the figures presented in the following sections, the TSR are not always exactly identical for all curves.

Table 5 summarises the rotation speed in RPM of the rotor for every tested velocity U_∞ and TSR. Some of the tests corresponding to this table were repeated several times in order to check particular tank characteristics (blockage effects, turbulence level, etc.).

TSR	U_∞ $[m/s]$			
	0.6	0.8	1.0	1.2
0.0	0.0	0.0	0.0	0.0
1.0	16.4	21.8	27.3	32.7
2.0	32.7	43.7	54.6	65.5
2.5	40.9	54.6	68.2	81.9
3.0	49.1	65.5	81.9	98.2
3.5	57.3	76.4	95.5	114.6
4.0	65.5	87.3	109.1	131.0
4.5	73.7	98.2	122.8	147.3
5.0	81.9	109.1	136.4	163.7
5.5	90.0	120.0	150.1	180.1
6.0	98.2	131.0	163.7	196.4
7.0	114.6	152.8	191.0	229.2

Table 5: RPM for every tested velocities U_∞ and TSR

2.5. Convergence accuracy tests

In order to check the convergence accuracy of the power and thrust coefficients, long acquisitions were recorded with a duration of $1000s$ at IFREMER and $600s$ at CNR-INSEAN flume tanks. Figures 8 and 9 present the time history of these coefficient during this long record obtained for $U_\infty = 0.8m/s$ and TSR = 3.0. These signals are calculated using equations 5 and 6 taking into account the time dependant torque M_x, rotation speed Ω and axial force F_x. The time history C_P and C_T are plotted in blue on these figures, whereas green points depict the local sliding $100s$ (or $60s$ for CNR-INSEAN 2) average. Horizontal histogram plots of these records show the probability density function of the mean (red line) and standard deviation (green lines) of these data.

In the towing tank, the acquisition time is always limited by the length of the tank. In order to allow comparisons with the circulating tank results present above, figures 10 and 11 presents the maximum acquisition time history for C_P and C_T coefficients, recorded during a full length run at $0.8m/s$ carriage speed, for KHL and CNR-INSEAN towing tanks respectively.

All statistical results are gathered in table 6, with average and standard-deviation (STD) values of C_P and C_T . Ratios between STD and average values are also given and expressed in %. The peak-to-peak value (P-to-P) is processed from the ratio between the highest difference of the local sliding $100s$ average (or $60s$ for CNR-INSEAN 2) and the mean of the whole signal. These last values are not available for KHL, because of the size of the tank which limits the acquisition time.

When comparing the results from the flume tanks (figures 8 and 9), it is clear that the standard-deviation is higher at IFREMER for C_P. According to table 6, this value is about two times higher than the one for CNR-INSEAN. The $100s$ sliding average (green points) shows larger fluctuations too, as shown by the peak-to-peak values for both C_P and C_T. This can be mainly explained by the difference of the flow turbulence intensity between the tanks.

Tank	P-to-P [%]		C_P			C_T		
	C_P	C_T	mean	STD	ratio [%]	mean	STD	ratio [%]
IFREMER	3.95	1.90	0.363	0.018	4.92	0.816	0.025	3.01
CNR-INSEAN 1	1.30	0.71	0.363	0.010	2.62	0.853	0.021	2.52
KHL	NA	NA	0.365	0.008	2.20	0.845	0.023	2.76
CNR-INSEAN 2	0.63	0.33	0.373	0.006	1.70	0.837	0.016	1.86

Table 6: Statistical results from long acquisition tests for C_P and C_T obtained for $U_\infty = 0.8m/s$ and TSR = 3.0.

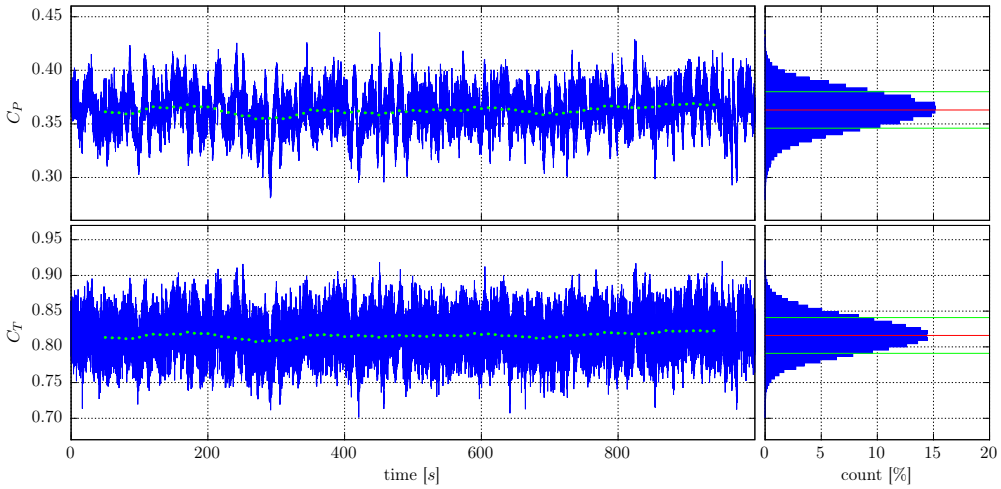

Figure 8: $1000s$ acquisition of C_P and C_T coefficients versus time, for $U_\infty = 0.8m/s$ and TSR = 3.0 recorded at IFREMER flume tank. Green points depict the $100s$ moving average of each signal. These signals are composed of 10^5 points with a data-rate of $100Hz$.

For towing tanks (figures 10 and 11), the standard-deviation of the C_P is lower than the values found in flume tanks. The difference is less marked for C_T with about the same value for KHL but a lower one for CNR-INSEAN (table 6). Standard-deviation values obtained for this tank are the lowest between the four experimental facilities.

Finally, according to these results, the standard acquisition time is $60s$ for the CNR-INSEAN towing tank and $100s$ for both flume tanks. For the KHL towing tank, the maximum acquisition time allowed by the length of the tank is chosen (table 2). However, compared to the other tanks, this acquisition time seems to be short to allow the mean of C_P and C_T to be totally converged (figure 10).

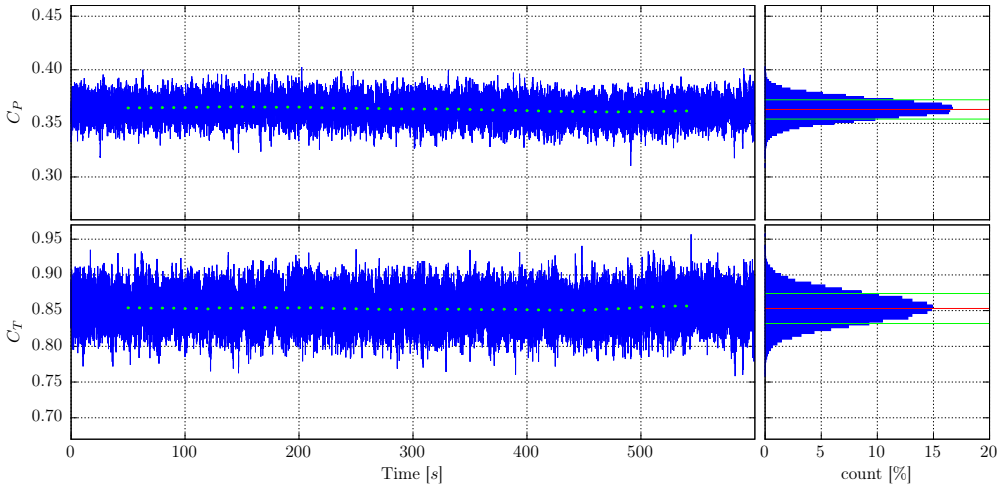

Figure 9: $10min$ acquisition of C_P and C_T coefficients versus time, for $U_\infty = 0.8m/s$ and TSR $= 3.0$ recorded at CNR-INSEAN flume tank. Green points depict the $100s$ moving average of each signal.

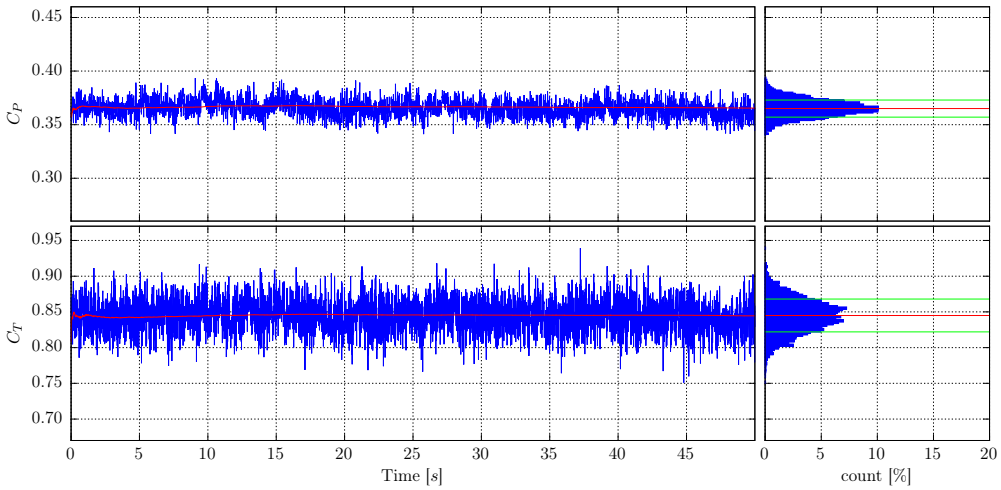

Figure 10: Maximum recorded time for C_P and C_T coefficients and for the carriage speed of $0.8m/s$ and TSR $= 3.0$, acquired at KHL towing tank. Red lines depict the time-related mean.

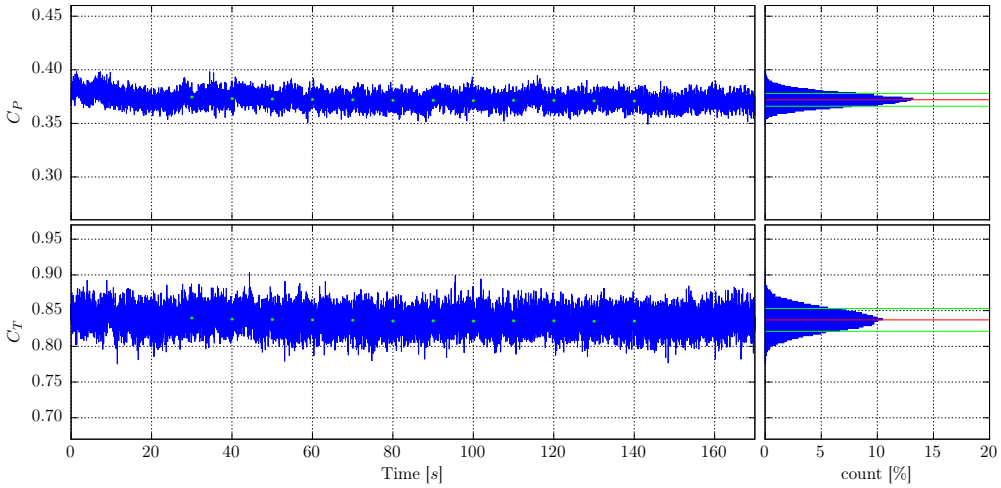

Figure 11: Maximum recorded time for C_P and C_T coefficients and for the carriage speed of $0.8m/s$ and TSR = 3.0, acquired at CNR-INSEAN towing tank. Green points depict the $60s$ moving average of each signals.

3. Performance evaluation

The first stage of the "Round Robin" programme took place in the IFREMER wave and current circulating tank in June 2013. The testing protocol (section 2.4) defined during this first leg of the "Round Robin" has been reproduced in the three other facilities. The same instrumentation has been used with the support of IFREMER staff so as to guarantee the repeatability of the measurement process. The second stage of the "Round Robin" testing took place at the University of Strathclyde in December 2013, while the third stage took place at CNR-INSEAN in April 2014. In this section, the results obtained in term of power and thrust coefficients are presented for $U_\infty = 1.0\ m/s$ only. The same results for the other speeds, $U_\infty = [0.6;\ 0.8;\ 1.2]\ m/s$ are shown in Appendix A. Flow measurements for wake characterization and blade deformation measurements have not been carried out in this study.

3.1. Power coefficient

Figure 12 presents the power coefficient obtained for $U_\infty = 1.0m/s$ in the four different tanks versus the TSR, in term of average and standard-deviation.

Some tests were repeated for every TSR and so, in some cases, several curves are available. In order to keep the following figures as clear as possible, the average and standard-deviation of these different curves have only been plotted here when repeats were carried out, so as to present only one curve per tank. So, the error-bars plotted on this figure show the dispersion of the different results obtained for identical configurations.

The average part of the figure shows a good agreement between the results obtained in the different tanks. Only slight differences are noticeable from TSR $\geqslant$ 2.5: the averaged C_P curves can be divided into two different groups with the IFREMER and KHL tanks

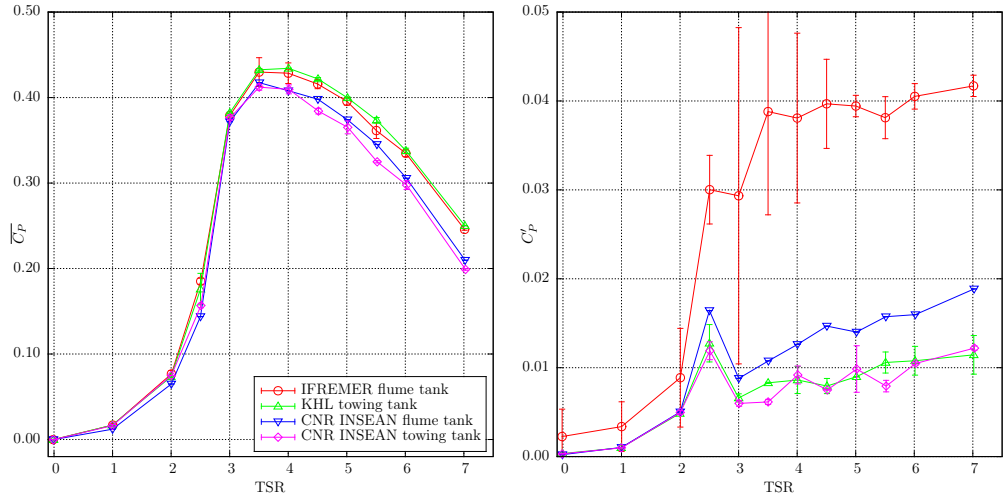

(a) $\overline{C_P}$ (b) C'_P

Figure 12: Mean and standard-deviation of the power coefficient obtained for every run at every tank for $U_\infty = 1.0m/s$

on one side with highest values and the CNR-INSEAN on the other side with lowest values.

Concerning the standard-deviation part, higher values are clearly remarkable for the IFREMER flume tank from TSR $\geqslant 2.5$. In addition, curves coming from the two towing tanks are grouped and the blue curve from the CNR-INSEAN flume tank starts to be detached from this group from TSR $\geqslant 2.5$ with slightly higher values.

3.2. Thrust coefficient

In the following section, thrust coefficients curves corresponding to previous power coefficient ones are plotted on figure 13, for the same flow or carriage speed of $1.0m/s$.

Identically to the power coefficient curves, all C_T curves are in good agreement between the tanks for the averaged part of the coefficient. However, two distinct groups can be observed with slight differences from TSR $\geqslant 2.5$: first one with the curves showing the highest values are for the KHL towing tank and the CNR-INSEAN flume tank, whereas the lowest values are obtained for the IFREMER flume tank and the CNR-INSEAN towing tank.

Three groups can be distinguished for the standard-deviation part of the figure. The first one showing the lower values comes from the CNR-INSEAN towing tank. Then, the CNR-INSEAN flume tank and KHL towing tank present values just slightly higher. And finally values coming from the IFREMER flume tank are increasing from TSR $\geqslant$ 3.5 to reach a maximum more than twice as high as the other tanks.

According to these results and those presented in Appendix A, it seems that the fluctuation part of these two coefficients C_P and C_T is mainly driven by the flow turbulence with the highest standard-deviation levels for the circulating tanks and the lowest ones obtained for the towing tanks.

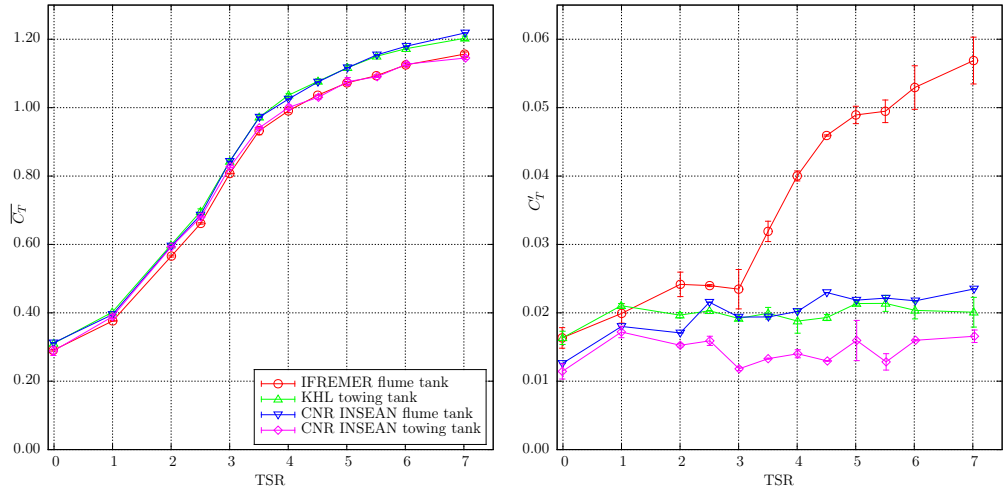

(a) $\overline{C_T}$ (b) C'_T

Figure 13: Mean and standard-deviation of the thrust coefficient obtained for every run at every tank for $U_\infty = 1.0m/s$

However, it is important to note that the differences in the standard deviations of the power and thrust cannot be explained only by differences in the turbulence intensity. The turbulence intensity is 3.0% at IFREMER and 2.5% at CNR-INSEAN, yet the standard deviations of power and thrust are in some cases twice as large. In order to investigate this discrepancy further, the flow turbulence should be charactered more fully, with reference to parameters such as turbulence length scales or dissipation rate (see [20]).

Concerning the average part of the power and thrust coefficients, blockage ratio effects coming from differences between tank sections (table 1) need to be investigated. This point is going to be studied in the following section.

4. Blockage effects

The impact of the effect of blockage was examined by applying the simplified blockage correction as suggested by [15]. This paper present an approach for correcting the results gathered in a tunnel (*i.e.* with no free surface) based on an actuator disc model. This correction attempts to reflect the increased thrust and power generated by a turbine in an enclosed tunnel due to the constriction of the wake behind the turbine. The actuator disc approach fails to capture some key aspects of the blockage on the flow physics, including the impact of blockage on details of the near-rotor vortex wake (see for example [21]) and neglects many aspects of the detailed geometry of the turbine in the tunnel such as the cross-section shape of the tunnel and the proximity of the turbine to flow boundaries. However, there is some experimental evidence to suggest that an actuator disc approach can represent the wake reasonably well far downstream (*e.g.* distance higher than three diameters) of the turbine even in relatively low turbulence inflow [22].

This approach calculates an equivalent free-stream velocity (U_F) based on the ratio of the turbine area to the tank or flume cross section area and the measured thrust coefficient. The ratio (U_T/U_F) of the measured velocity (U_T) to the equivalent free-stream velocity is used to correct the tip speed ratio; the square and cube of this ratio are used to correct the thrust and power coefficients respectively. The blockage corrections for power thus obtained are shown for the four facilities in figure 14.

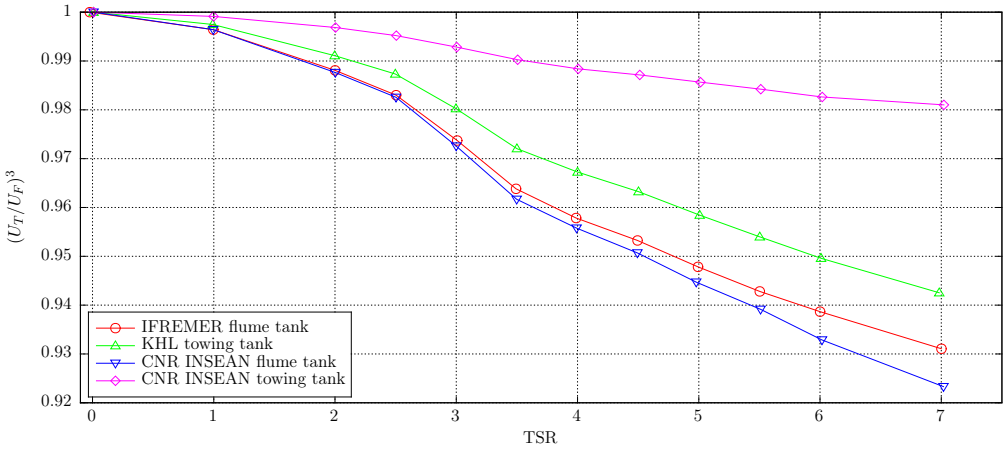

Figure 14: Blockage correction for power coefficient for the four facilities

The magnitude of the corrections are not so different for the IFREMER flume, the KHL towing tank and the CNR-INSEAN flume. Consequently application of this correction does not significantly affect the comparison between results obtained from these three facilities, and the differences between the results from these three facilities cannot be explained by blockage effects. However the blockage correction for the much larger CNR-INSEAN towing tank is significantly different from the other three facilities, and consequently the results after application of the blockage correction for the CNR-INSEAN tank are much closer to those from the other three facilities. This is illustrated in figures 15 for the curves of averaged power and thrust coefficients at $U_\infty = 1m/s$ and in Appendix B at all other speeds.

As shown in the previous section but also in Appendix A, averaged C_P and C_T values are generally higher when the blockage ratio increases. This corresponds to the uncorrected curves presented on figures 12a and 13a (or A.17a to A.22a) where red or green curves coming from IFREMER and KHL are mostly at the top part of the point cloud, whereas the pink curves from the widest and deepest tank of CNR-INSEAN are often lower.

On the contrary, on figures 15 and in Appendix B, the curves are clearly in better agreement. Comparing to the uncorrected data, points from IFREMER, KHL and CNR-INSEAN flume tank are lower thanks to the blockage correction, whereas those from the CNR-INSEAN towing tank are essentially identical.

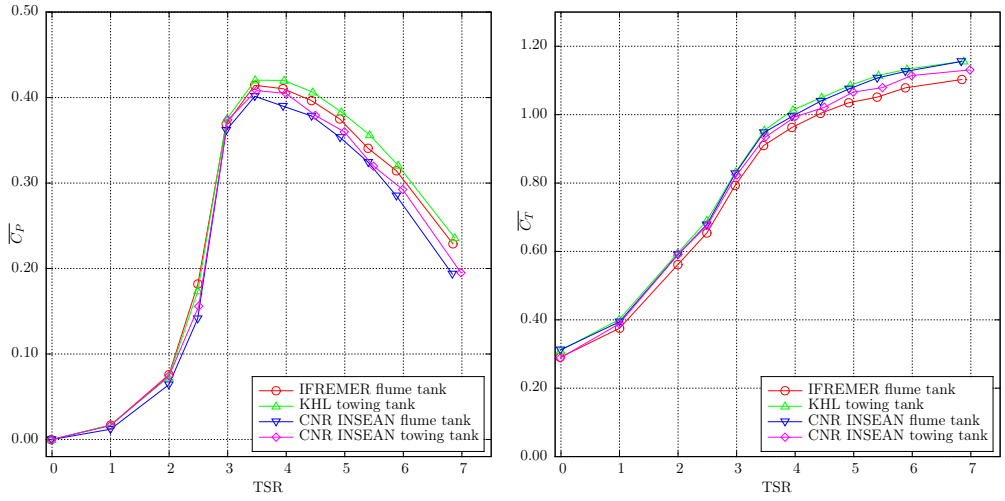

(a) $\overline{C_P}$ (b) $\overline{C_T}$

Figure 15: Average of the power and thrust coefficients obtained for every run at every tank for $U_\infty = 1.0m/s$ with blockage correction

A number of authors (*e.g.* [23]) imply that blockage corrections are unnecessary when blockage area ratios are less than 5%. These results show that this assumption may not be reliable for prediction of power coefficient at high TSR for which thrust coefficients are high.

However some differences remain. For example, KHL towing tank continues to yield larger C_T and also sometimes larger C_P values; slight oscillations of the towing carriage combined with excitation of a set-up natural frequency can create vibrations of the mast. These oscillations increase the drag force on the structure and thus the thrust coefficient (*e.g.* see figure A.20 at $U_\infty = 0.6m/s$) which is processed in this study from the total drag force acting on the whole structure, as explained in section 2.3. As shown in section 2.5, the acquisition time may also be responsible for some few percent of variation: 0.3 to close to 4% depending on the tanks, from peak-to-peak results. In addition, flow velocities (or accuracy of the carriage speeds) were not measured during these tests; as shown by [20], power and thrust measurements are strongly sensitive to the estimation of the ambient velocity for flume tanks.

A further aspect needs to be studied in order to explain the differences between the average results: the turbulence effects, knowing that different turbulent inflow regimes can be encountered especially in flume tanks comparing to towing tanks. It has already been shown in section 3 and Appendix A that the turbulence intensity has a strong impact on the fluctuation part of the coefficients, but it may be also the case for the average part.

5. Reynolds effects

In all facilities, the turbine performance shows a trend to improve at increasing testing velocity. An explanation of this behaviour can be provided by considering the chord-based Reynolds number at $r/R = 0.7$, commonly used in propeller design and shown in equation 7.

$$Re_{0.7} = \frac{c_{0.7}\sqrt{U_\infty^2 + (0.7R\,\Omega)^2}}{\nu} \tag{7}$$

where $c_{0.7}$ is the blade chord length at $r/R = 0.7$.

This number can be used to identify the flow regimes encountered by the rotor blade at different TSR. Normally in rotor design, the section at $r/R = 0.7$ is considered to be representative of the loading condition of the blade and the section where the maximum lift circulation is achieved.

On figure 16 are shown the fitted curves of the averaged C_P (dashed lines) for IFREMER flume tank, versus $Re_{0.7}$ for the tested velocity. In addition, the corresponding maximum $\overline{C_P}$ are plotted with solid lines, for all facilities. The improvement of turbine performance with the $Re_{0.7}$ is clearly highlighted independently by the considered facility. The justification of the above behaviour lies in the low $Re_{0.7}$, for the adopted model turbine. In fact $Re_{0.7}$ is in the range $3.10^4 - 3.10^5$ which is quite critical for the performance at stall (maximum of the lift coefficient C_L, post-stall response) for the rotor blade sections.

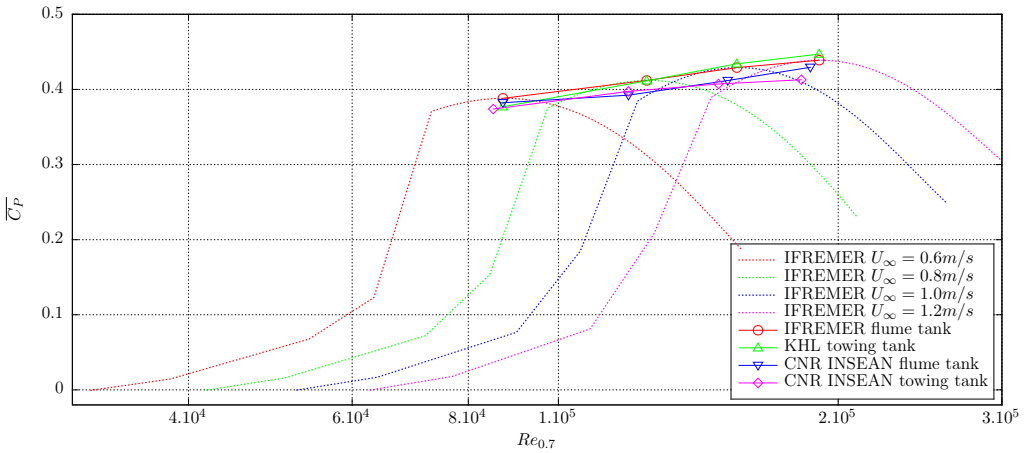

Figure 16: Dashed lines stand for the fitted curves of the averaged C_P coefficients for IFREMER flume tank, versus $Re_{0.7}$ and for every tested velocities. Maximum of these curves are plotted with solid lines and for every facilities.

In fact wing sections within this regime show laminar boundary layer on the low pressure side of the foil that is susceptible to separation due to the adverse pressure gradient, resulting in a loss in hydrodynamic performances and unstable lift and premature stall [24]. Furthermore [25] showed that such phenomena is very apparent for thick foils,

such as the NACA 63-418 adopted in the present turbine, which is subject to critical transition regimes for $3.10^4 < Re_{0.7} < 5.10^5$. Performance of the wing section clearly improves with the Reynolds number. This is due to laminar to turbulent transition of the boundary layer on the suction side of the wing section that delays the flow detachment on the suction side of the foil. Consequently the same behaviour also occurs for the turbine performance for all TSR.

In the C_P plots, at the lowest velocity ($U_\infty = 0.6m/s$), the flow regime in the blade boundary layer is laminar, due to the very low $Re_{0.7}$, with the consequence that for all the facilities the curve collapse together. However at higher speed a spread between all facilities can be observed in figure 16. One important contribution to these differences is probably due to the inflow turbulence of the different facilities which affects the hydrodynamic performance of the turbine. In fact as shown by [26] and [27] for foil sections, the chief effect of inflow turbulence is to destabilize the laminar boundary layer and force transition sooner than it would otherwise occur. The turbulent boundary layer is thus more extensive; as a consequence its capability in remaining attached against the adverse pressure gradient provides higher performances. Consequently at low Reynolds numbers, free stream turbulence can increase the maximum lift coefficient beyond what it would be in smooth flow. Following the previous considerations, it is apparent in figure 16 that the facilities with higher inflow turbulence achieve higher turbine performance. For the KHL towing tank, some carriage vibration can be considered to have an effect which may be equivalent to the turbulent inflow in the flume facilities.

However previous studies performed for two different turbulence intensities (3 and 15%) at the IFREMER flume tank [16] do not allow a generalization of the assumption that in the same facility, performances are higher with an incoming flow with 15% turbulence intensity than with a 3% turbulence intensity flow. It is likely that a better characterization of the turbulence inflow, also in term of frequency and scale distribution is necessary to fully and accurately investigate that point [20].

For flume facilities, the acquisition time is fixed at $100s$. According to section 2.5, this can create variations of the averaged power coefficient of 3.95% and 1.30% (peak-to-peak values) for the IFREMER and CNR-INSEAN tanks respectively, which are significant. In a towing tank, the waiting time between two consecutive runs can also influence the results in an unpredictable manner, even when care is taken during the tests. This effect may be directly linked with the fluctuating parts of the power and thrust coefficients, shown on section 3, which increase with the turbulence intensity of the incoming flow or vibrations of the towing tank carriage.

As shown by all of these previous results, the turbulence intensity and the turbulent inflow regime (depicted here by the chord-based Reynold number) play a significant role in the performances of a marine turbine.

6. Conclusions and Future Work

A "Round Robin" testing program has been conducted in wich the same tidal turbine model was tested in four different experimental facilities, comprising two towing tanks and two circulating flow tanks. Performance assessments based on measurement of torque, drag and inflow speed show very similar results for the three-bladed horizontal axis marine turbine tested.

The greatest variations between results from different facilities are found in measures of the time-varying fluctuations of the power and thrust coefficients. It is believed that these results principally come from the differences in the turbulent inflow in the circulating tanks or from carriage vibrations in the towing tanks. Slight variations are observed on the time-mean values of these coefficients, especially at higher TSR. In this regard, two different aspects are discussed in this paper: the blockage effect and the turbulent inflow regime.

The blockage effect correction coefficients calculated in this study based on [15] mainly affect the prediction of power coefficient at high TSR when thrust coefficients are high. The value of this correction coefficient found for the highest power coefficient, at TSR close to 4, is less than 5% for all the facilities used here. In parallel, the precision of the time-mean values of the power coefficient varies with the same proportions with the $100s$ duration acquisition time, when the turbine is in the turbulent incoming flow of the IFREMER circulating tank.

The level of incoming flow turbulence in the different test facilities clearly affects the performance of the turbine. More generally, improved understanding and modelling of this effect is of great importance in order to improve testing methodology for model-scale marine current turbine, especially with regard to performance assessments of the full-scale devices. Principally, two main issues need to be studied in more detail:

1. The turbulence of the incoming flow is currently not adequately described. Researchers usually give a brief description of the incoming flow, characterising turbulence only by intensity. However integral length scale also affects performance, as shown by [7], who demonstrate that drag forces on a porous disc are dependent not only on turbulence intensity but also on integral length scale. A similar study is necessary for a rotating turbine in order to examine this issue with regard to the power coefficient curve.

2. The Reynolds number in the model tests is very different from the full-scale turbine. The importance of Reynolds number effects has been extensively studied in aeronautics and for marine propellers. The section drag and lift coefficients are strongly dependent on this number, especially because blade sections are close to the stall angle in the working conditions of the turbine. Higher rotation speeds and flow velocities are necessary to increase the Reynolds number; however this can be difficult to achieve in many testing facilities. Approaches such as boundary layer tripping or modification of the turbulence characteristics of the flow can be deployed experimentally to force the boundary layer transition in the fluid. However, these approaches require validation in order to be used with confidence. Numerical models, including Boundary Elements Momentum models as well as CFD approaches, may help to develop further understanding of this issue.

Acknowledgement

The authors gratefully acknowledge the EU for the financial support granted for financed the MaRINET Initiative under the FP7 "Capacities" Specific Programme through grant agreement number 262552, MaRINET.

We also would like to thank Thomas Bacchetti, Tom Mc Combes, Katie Gracie and Francesco Salvatore for their assistance in this experimental work.

References

[1] M. Healy, T. Lewis, R. Alcorn, MARINET - Streamlined, free-of-charge access to test facilities: How world-class research centres are joining forces to accelerate the development of marine renewable energy, 4th International Conference on Ocean Energy (ICOE), Dublin, Ireland, 2012.

[2] J. Bard, J.-B. Richard, J.-M. Rousset, B. Elsässer, E. R. Sestafe, M. Finn, L. Johanning, Research activities in the MaRINET project: Keeping the European marine energy development facilities at world top level, 4th International Conference on Ocean Energy (ICOE), Dublin, Ireland, 2012.

[3] C. M. Johnstone, T. McCombes, A. S. Bahaj, L. Myers, B. Holmes, J. P. Kofoed, C. Bittencourt, EquiMar: Development of Best Practices for the Engineering Performance Appraisal of Wave and Tidal Energy Converters, 9th European Wave and Tidal Energy Conference (EWTEC), Southampton, UK, 2011.

[4] Specialist Committe on testing of Marine Renewable Devices, ITTC Recommended Guidelines - Model Tests for Current Turbines, Tech. Rep. 7.5-02-07-03.9, 27th International Towing Tank Conference (ITTC), Copenhagen, Denmark (2014).

[5] L. E. Myers, A. S. Bahaj, Experimental analysis of the flow field around horizontal axis tidal turbines by use of scale mesh disk rotor simulators, Ocean Engineering 37 (2 - 3) (2010) 218 – 227. doi:10.1016/j.oceaneng.2009.11.004.

[6] L. E. Myers, A. S. Bahaj, An experimental investigation simulating flow effects in first generation marine current energy converter arrays, Renewable Energy 37 (1) (2012) 28 – 36. doi:10.1016/j.renene.2011.03.043.

[7] T. Blackmore, W. M. J. Batten, G. U. Müller, A. S. Bahaj, Influence of turbulence on the drag of solid discs and turbine simulators in a water current, Experiments in Fluids 55 (1). doi:10.1007/s00348-013-1637-9.

[8] T. Stallard, R. Collings, T. Feng, J. Whelan, Interactions between tidal turbine wakes: experimental study of a group of three-bladed rotors, Philosophical Transactions of the Royal Society A: Mathematical, Physical and Engineering Sciences 371 (1985). doi:10.1098/rsta.2012.0159.

[9] S. Tedds, R. Poole, I. Owen, G. Najafian, S. Bode, A. Mason-Jones, C. Morris, T. O'Doherty, D. O'Doherty, Experimental investigation of horizontal axis tidal stream turbine, 9th European Wave and Tidal Energy Conference (EWETEC), Southampton, UK, 2011.

[10] I. Milne, A. Day, R. Sharma, R. Flay, Blade loads on tidal turbines in planar oscillatory flow, Ocean Engineering 60 (2013) 163 – 174. doi:10.1016/j.oceaneng.2012.12.027.

[11] P. Davies, G. Germain, B. Gaurier, A. Boisseau, D. Perreux, Evaluation of the durability of composite tidal turbine blades, Philosophical Transactions of the Royal Society A: Mathematical, Physical and Engineering Sciences 371 (1985). doi:10.1098/rsta.2012.0187.

[12] B. Gaurier, P. Davies, A. Deuff, G. Germain, Flume tank characterization of marine current turbine blade behaviour under current and wave loading, Renewable Energy 59 (2013) 1 – 12. doi:10.1016/j.renene.2013.02.026.

[13] G. Pinon, P. Mycek, G. Germain, E. Rivoalen, Numerical simulation of the wake of marine current turbines with a particle method, Renewable Energy 46 (2012) 111 – 126. doi:10.1016/j.renene.2012.03.037.

[14] P. Mycek, B. Gaurier, G. Germain, G. Pinon, E. Rivoalen, Numerical and experimental study of the interaction between two marine current turbines, International Journal of Marine Energy 1 (2013) 70 – 83. doi:10.1016/j.ijome.2013.05.007.

[15] A. S. Bahaj, A. F. Molland, J. R. Chaplin, W. M. J. Batten, Power and thrust measurements of marine current turbines under various hydrodynamic flow conditions in a cavitation tunnel and a towing tank, Renewable Energy 32 (3) (2007) 407 – 426. doi:10.1016/j.renene.2006.01.012.

[16] P. Mycek, B. Gaurier, G. Germain, G. Pinon, E. Rivoalen, Experimental study of the turbulence intensity effects on marine current turbines behaviour. Part I: One single turbine, Renewable Energy 66 (2014) 729 – 746. doi:10.1016/j.renene.2013.12.036.

[17] G. Germain, Marine current energy converter tank testing practices, 2nd International Conference on Ocean Energy (ICOE), Brest, France, 2008.

[18] I. H. Abbott, A. E. Von Doenhoff, Theory of Wing Sections, Including a Summary of Airfoil Data, Dover Books on Aeronautical Engineering Series, Dover Publications Inc., 1959.

[19] P. Mycek, B. Gaurier, G. Germain, G. Pinon, E. Rivoalen, Experimental study of the turbulence intensity effects on marine current turbines behaviour. Part II: Two interacting turbines, Renewable Energy 68 (2014) 876 – 892. doi:10.1016/j.renene.2013.12.048.

[20] T. Blackmore, B. Gaurier, L. Myers, G. Germain, A. Bahaj, Turbulence and Tidal Turbines, 11th European Wave and Tidal Energy Conference (EWETEC) IN PRESS, Nantes, FR, 2015.

[21] S. McTavish, D. Feszty, F. Nitzsche, An experimental and computational assessment of blockage effects on wind turbine wake development, Wind Energy 17 (10) (2014) 1515 – 1529. doi:10.1002/we.1648.

[22] S. Aubrun, S. Loyer, P. Hancock, P. Hayden, Wind turbine wake properties: Comparison between a non-rotating simplified wind turbine model and a rotating model, Journal of Wind Engineering and Industrial Aerodynamics 120 (2013) 1 – 8. doi:10.1016/j.jweia.2013.06.007.

[23] J. I. Whelan, J. M. R. Graham, J. Peiró, A free-surface and blockage correction for tidal turbines, Journal of Fluid Mechanics 624 (2009) 281 – 291. doi:10.1017/S0022112009005916.

[24] P. B. S. Lissaman, Low-reynolds-number airfoils, Annual Review of Fluid Mechanics 15 (1983) 223–239. doi:10.1146/annurev.fl.15.010183.001255.

[25] T. J. Mueller, S. M. Batil, Experimental studies of separation on a two-dimensional airfoil at low reynolds numbers, American Institute of Aeronautics and Astronautics Journal 20 (4) (1982) 457–463. doi:10.2514/3.51095.

[26] P. Devinant, T. Laverne, J. Hureau, Experimental study of wind-turbine airfoil aerodynamics in high turbulence, Journal of Wind Engineering and Industrial Aerodynamics 90 (6) (2002) 689 – 707. doi:10.1016/S0167-6105(02)00162-9.

[27] E. N. Jacobs, A. Sherman, Airfoil section characteristics as affected by variations of the Reynolds number, Tech. Rep. 586, National Advisory Committee for Aeronautics (1937).

Appendix A. Performance evaluation - raw data

Appendix A.1. Power coefficient

Figures A.17 to A.19 present the power coefficient in terms of mean and standard-deviation for every tank and for the three velocities $U_\infty = [0.6; 0.8; 1.2] m/s$, without blockage effect corrections.

Concerning the averaged C_P curve, differences between tanks are negligible for the smallest velocity, but appear for 0.8 and $1.2 m/s$ for TSR $\geqslant 3$. The highest values are obtained for the IFREMER and KHL tanks, whereas the smallest ones come from the CNR-INSEAN towing tank. This is linked to the blockage ratio: *i.e.* the highest blockage ratio shows the highest power coefficient values.

The fluctuation part of the power coefficient is higher for the IFREMER flume tank, for every velocity and from TSR $\geqslant 2$. Smaller fluctuations are measured for the two towing tanks. This is directly linked to the turbulence in the flow: the higher the turbulence and the higher the fluctuations.

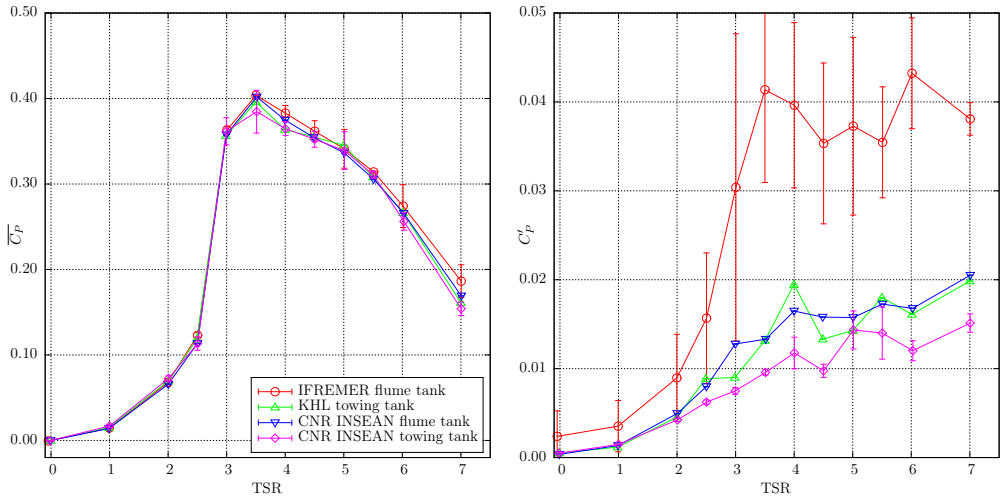

(a) $\overline{C_P}$ (b) C'_P

Figure A.17: Mean and standard-deviation of the power coefficient obtained for every run at every tank for $U_\infty = 0.6 m/s$

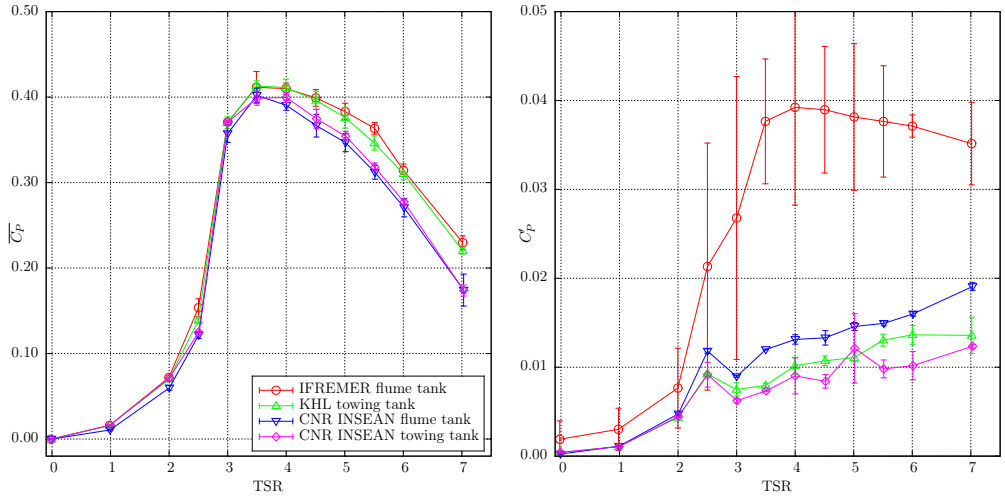

(a) $\overline{C_P}$ (b) C'_P

Figure A.18: Mean and standard-deviation of the power coefficient obtained for every run at every tank for $U_\infty = 0.8m/s$

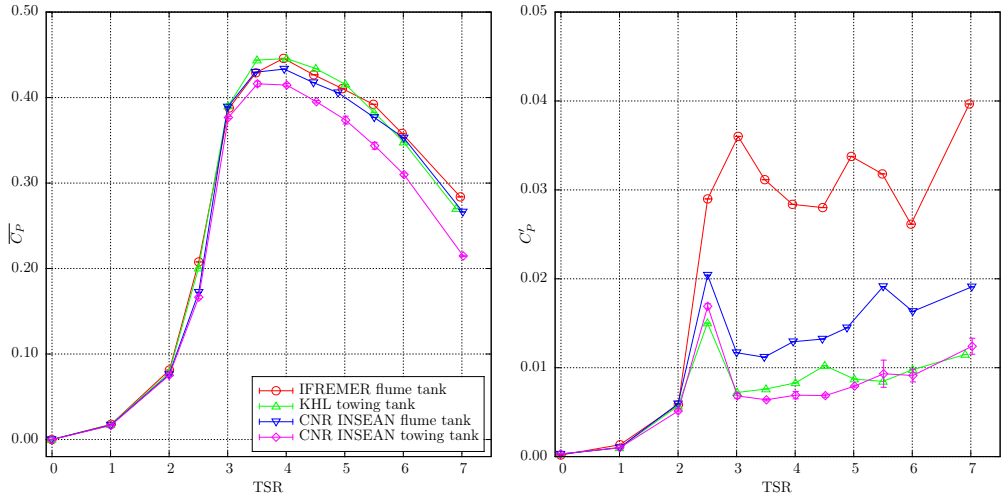

(a) $\overline{C_P}$ (b) C'_P

Figure A.19: Mean and standard-deviation of the power coefficient obtained for every run at every tank for $U_\infty = 1.2m/s$

Appendix A.2. Thrust coefficient

Figures A.20 to A.22 show the thrust coefficient curves obtained for $U_\infty = [0.6; 0.8; 1.2] m/s$ and for all tanks, without blockage effect corrections.

The average part of the thrust coefficients show good agreement between the different tanks. Some slight differences appear however from TSR $\geqslant 2.5$ with lower values obtained for the IFREMER flume and the CNR-INSEAN towing tank. Higher values are measured for the KHL towing tank and the CNR-INSEAN flume tank. For $U_\infty = 0.6 m/s$, average measurements and fluctuation levels are higher for the KHL tank than for the others because of weak vibrations on the mast. These vibrations increase the fluctuations in thrust as well as the mean drag on the mast (and thus the thrust).

Except for this particular case, the standard-deviation of the thrust coefficient is similar to the one obtained for the power coefficient. The highest values are measured at IFREMER and the lowest are observed at the CNR-INSEAN towing tank. Again, this follows the flow turbulence intensity.

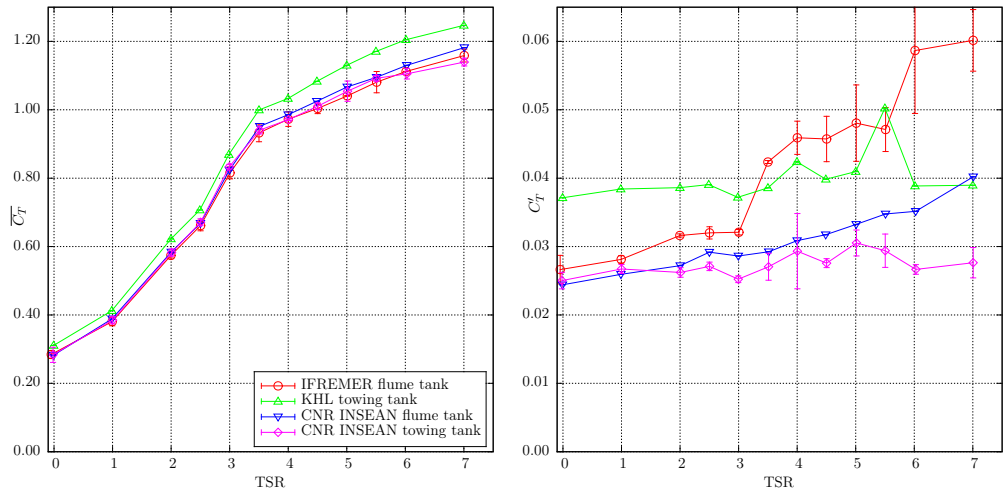

(a) $\overline{C_T}$ (b) C'_T

Figure A.20: Mean and standard-deviation of the thrust coefficient obtained for every run at every tank for $U_\infty = 0.6 m/s$

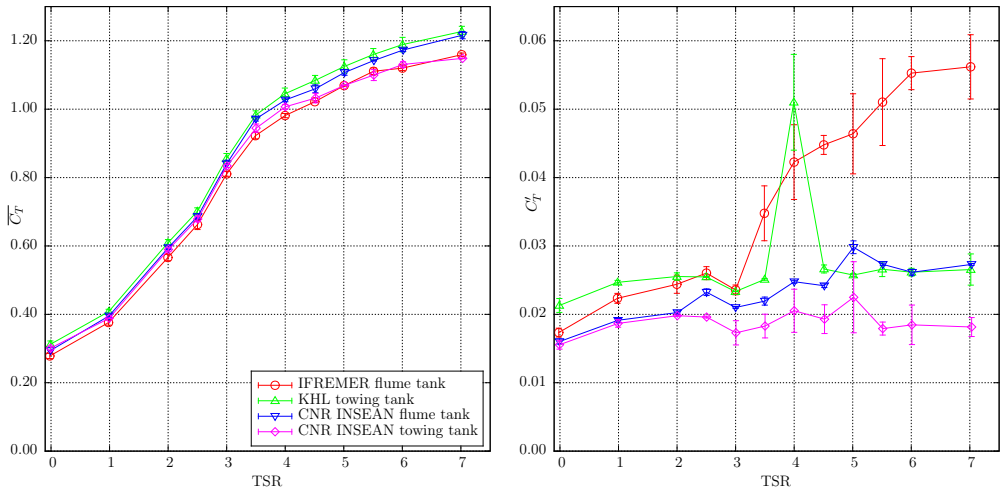

(a) $\overline{C_T}$ (b) C'_T

Figure A.21: Mean and standard-deviation of the thrust coefficient obtained for every run at every tank for $U_\infty = 0.8m/s$

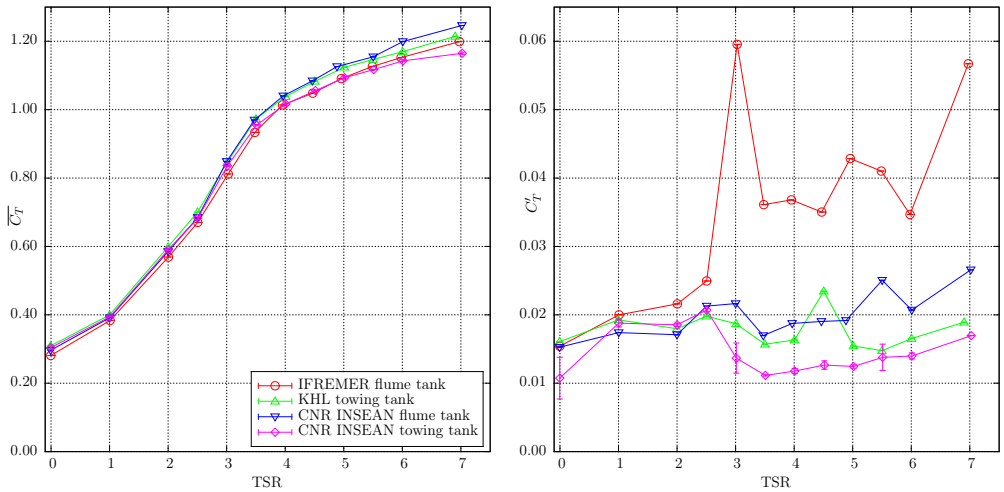

(a) $\overline{C_T}$ (b) C'_T

Figure A.22: Mean and standard-deviation of the thrust coefficient obtained for every run at every tank for $U_\infty = 1.2m/s$

Appendix B. Performance evaluation - corrected data

Figures B.23 to B.25 show the averaged power and thrust coefficient curves obtained for $U_\infty = [0.6; 0.8; 1.2]m/s$ and for all tanks, taking into account the blockage effect corrections (see section 4 for details).

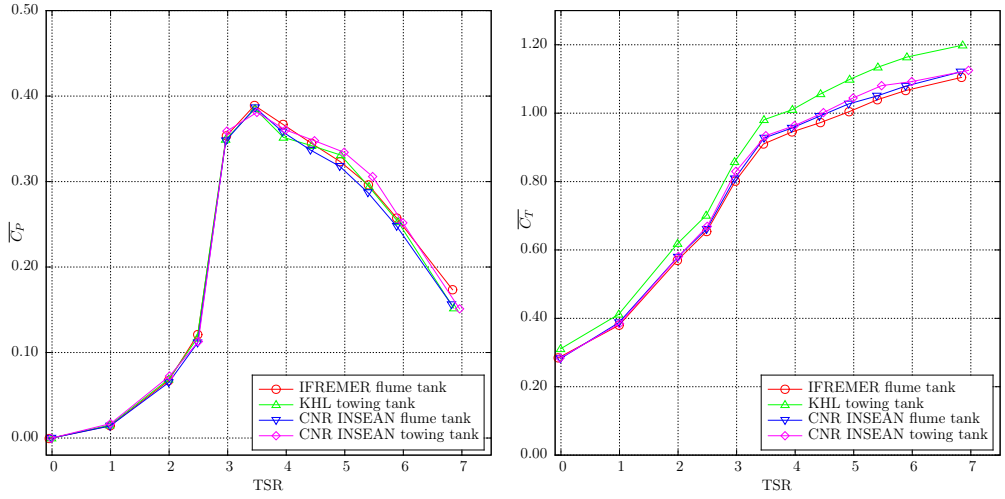

(a) $\overline{C_P}$ (b) $\overline{C_T}$

Figure B.23: Average of the power and thrust coefficients obtained for every run at every tank for $U_\infty = 0.6m/s$ with blockage correction

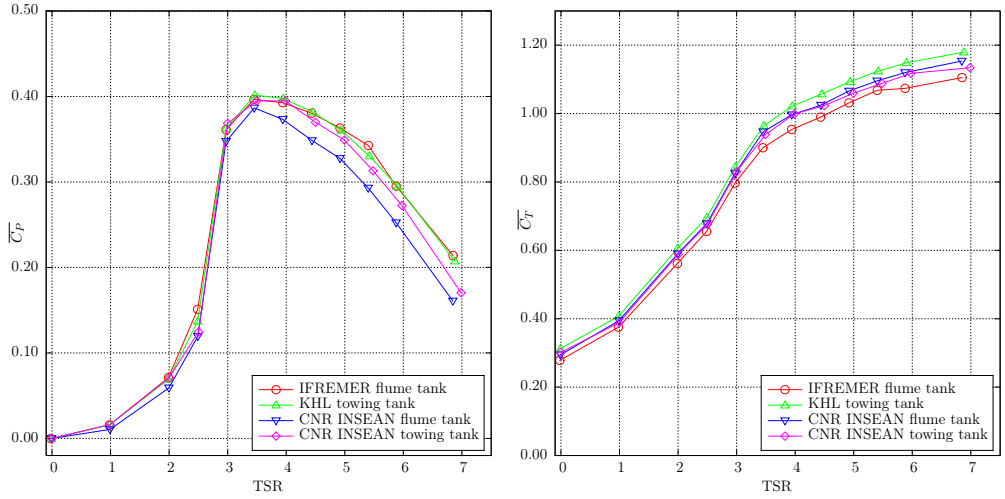

(a) $\overline{C_P}$ (b) $\overline{C_T}$

Figure B.24: Average of the power and thrust coefficients obtained for every run at every tank for $U_\infty = 0.8m/s$ with blockage correction

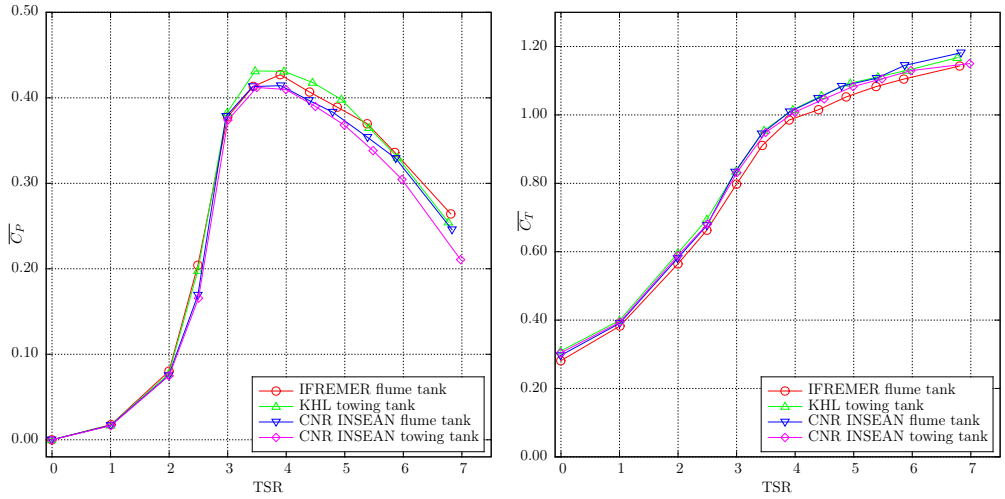

(a) $\overline{C_P}$ (b) $\overline{C_T}$

Figure B.25: Average of the power and thrust coefficients obtained for every run at every tank for $U_\infty = 1.2m/s$ with blockage correction